Title
A novel boundary element formulation for anisotropic fracture mechanics

Authors
Gulizzi, V
Benedetti, I
Milazzo, A

Publication Date
2019-12-01

DOI
10.1016/j.tafmec.2019.102329

Peer reviewed

A novel boundary element formulation for anisotropic fracture mechanics

Vincenzo Gulizzi[a], Ivano Benedetti[a], Alberto Milazzo[a,*]

[a] *Department of Engineering, University of Palermo, Viale delle Scienze, Edificio 8, Palermo, 90128, Italy.*

Abstract

A novel boundary element formulation for two-dimensional fracture mechanics is presented in this work. The formulation is based on the derivation of a supplementary boundary integral equation to be used in combination with the classic displacement boundary integral equation to solve anisotropic fracture mechanics problems via a single-region approach. The formulation is built starting from the observation that the displacement field for an anisotropic domain can be represented as the superposition of a vector field, whose components satisfy a suitably defined anisotropic Laplace equation, and the gradient of the Airy stress function. The supplementary boundary integral equation is then obtained using such representation into the integral expression of the aforementioned Laplace equation and employing the relationship between the stress function gradient and the boundary tractions. The supplementary equation neither requires the computation of hyper-singular integrals nor does it introduce additional variables for the problem, as it involves boundary displacements and tractions only. Numerical results are obtained for both uncracked and cracked bodies and show the accuracy and potential of the proposed approach.

Keywords: Fracture Mechanics, Anisotropic Elasticity, Integral Equations, Dual Boundary Element Method

*Corresponding author

Email addresses: `vincenzo.gulizzi@unipa.it` (Vincenzo Gulizzi), `ivano.benedetti@unipa.it` (Ivano Benedetti), `alberto.milazzo@unipa.it` (Alberto Milazzo)

1. Introduction

Fracture mechanics is nowadays a well established discipline, comprising a broad array of methodologies that support engineers in the design and maintenance of materials and structures. In general, the solution of fracture mechanics problems is obtained using numerical methods that allow to tackle the complexities induced by the occurrence of general boundary conditions or constitutive material behaviours.

One of the most popular numerical methods for addressing fracture mechanics and elasticity problems is the Finite Element Method (FEM). A powerful extension of the FEM for fracture mechanics applications is the Extended Finite Element Method, dubbed as XFEM [1, 2, 3], in which the approximation of the unknown field, namely the displacement field, is suitably enriched to account for the presence of the crack, representing a strong field discontinuity. However, both FEM and XFEM require the discretisation of the whole domain to be analysed and therefore a careful pre-processing mesh preparation stage.

A valid alternative technique for general elasticity and fracture mechanics applications is the Boundary Element Method (BEM), which reformulates such classes of problems in terms of boundary variables only [4, 5], thus leading to simpler pre-processing and lower numbers of degrees of freedom.

In fracture mechanics, however, the BEM modelling of geometrically coincident crack surfaces requires specific treatment, as the straightforward collocation of the displacement

boundary integral equations to geometrically superimposed but physically distinct nodes leads to numerical degeneracies not allowing to resolve the presence of crack [5].

To address such an issue several different techniques have been proposed in the literature. One of the earliest approaches was the use of specific Green's functions that intrinsically account for the presence of the crack in the domain and avoid the discretisation the crack itself [6, 7, 8]; however such a technique is based on the knowledge of different Green's functions for different crack geometries, which in many cases are difficult, if not impossible, to evaluate. Another powerful and versatile approach for modelling cracked domains using the BEM is the multi-region technique, which is based on a subdivision of the domain into subregions whose boundaries contain the crack [9, 10, 11]. Then, to retrieve the behaviour of the original domain, continuity/equilibrium interface conditions are enforced on the newly introduced boundaries, whereas traction-free boundary conditions are enforced over the crack surfaces. Advanced applications of such an approach, used in conjunction with cohesive zone modelling, have been developed for materials micro-mechanics [12, 13, 14, 15, 16]. However, multi-region formulations have the disadvantage of requiring a higher discretisation effort and introducing additional displacement and traction unknowns along the additional fictitious boundaries.

As opposed to the multi-region method, the so-called Dual Boundary Element Method (DBEM) has been developed by Aliabadi and coworkers [17, 18] as a single-region technique for fracture mechanics. The DBEM is based on the use of the standard displacement

boundary integral equation on one boundary of the crack and the traction boundary integral equation on the other boundary of the crack. The DBEM has been successfully employed for fracture mechanics problems in anisotropic elasticity [19, 20], dynamics [21], thermoelasticity [22, 23], and has been recently combined with the multi-region approach and the cohesive-law technique to model fracture micro-mechanics in polycrystalline materials [24, 25].

An alternative DBEM has been proposed by Davì and Milazzo [26, 27] for isotropic and orthotropic materials. The methodology consists of two steps: *i*) the displacement field is first represented as the linear superposition of a vector field, whose components satisfy a suitably defined Laplace equation, and the gradient of the Airy stress function; *ii*) this decomposition is then used within the integral representation of the mentioned Laplace equation and, by using the relationship between the gradient of the stress functions and the boundary tractions, a supplementary integral equation is obtained, to be used in conjunction with the classical displacement integral equation for avoiding the degeneracies arising in cracks modelling with standard BEM. The supplementary equation does not involve hyper-singular integrals and it has been used to solve single-region fracture problems in isotropic and orthotropic domains.

In this work, we revisit the approach proposed by Davì and Milazzo and extend it to the generally anisotropic case. More specifically: *i*) it is shown that a representation of the displacement field similar to the mentioned one can be used also in the anisotropic

case; *ii*) then, a supplementary integral equation is obtained after introducing such a decomposition into the integral representation of a suitably introduced anisotropic Laplace equation. The obtained integral equation for anisotropic elasticity keeps the same features as those obtained for the isotropic and orthotropic cases and and it is used for solving fracture mechanics problems in generally anisotropic bodies.

The paper is organised as follows: Section (2) introduces the classic displacement boundary integral equations; Section (3) and Section (4) are devoted to the derivation of the displacement decomposition and to the derivation of the supplementary boundary integral equation, respectively, whereas the application of the proposed formulation in the context of fracture mechanics is presented in Section (5). Section (6) discusses a few details of the numerical discretisation of the proposed method and Section (7) presents the performed numerical tests on both uncracked and cracked domains. Section (8) draws the study conclusions.

2. Displacement boundary integral equations

Let us consider a two-dimensional generally anisotropic linear elastic domain V with boundary $S = \partial V$. The boundary integral representation of the displacement field at a point $\boldsymbol{x}_0 = \{x_0, y_0\} \in S$ is classically given as follows [5]

$$\widehat{\boldsymbol{c}}(\boldsymbol{x}_0)\boldsymbol{u}(\boldsymbol{x}_0) + \fint_S \boldsymbol{T}(\boldsymbol{x}, \boldsymbol{x}_0)\boldsymbol{u}(\boldsymbol{x})\mathrm{d}S(\boldsymbol{x}) = \int_S \boldsymbol{U}(\boldsymbol{x}, \boldsymbol{x}_0)\boldsymbol{t}(\boldsymbol{x})\mathrm{d}S(\boldsymbol{x}), \tag{1}$$

where $\boldsymbol{u} = \{u_x, u_y\}$ and $\boldsymbol{t} = \{t_x, t_y\}$ denote the displacement and traction fields at the boundary of V respectively and $\widehat{\boldsymbol{c}}(\boldsymbol{x}_0)$ is a 2×2 matrix of the free terms, which depend

on the smoothness of the boundary S at $\boldsymbol{x}_0$. In Eq. (1), $\boldsymbol{U}(\boldsymbol{x}, \boldsymbol{x}_0)$ and $\boldsymbol{T}(\boldsymbol{x}, \boldsymbol{x}_0)$ are 2×2 matrices containing the components of the displacement and traction fundamental solutions respectively; their expressions for non-degenerate anisotropic and for degenerate isotropic materials [28] can be found in [4, 5].

Eq.(1) represents the starting point for the boundary element implementation and it has been widely employed to model general elasticity problems. However, it is well known that Eq.(1) does not allow to represent the presence of cracks within the considered domain using a single-region approach [5]. To overcome this limitation, Aliabadi and co-workers [17, 18] introduced the so-called Dual Boundary Element Method, where a supplementary integral equation is used in combination with the displacement boundary integral equation (1). The supplementary equation is obtained by deriving the integral representation of the boundary tractions $\boldsymbol{t}$ and involves the evaluation of hyper-singular integrals. In what follows, we present the derivation of an alternative additional integral equation that avoids the computation of hyper-singular integrals.

3. Displacement decomposition

In this Section, we derive a representation of the displacement field $\boldsymbol{u}$ in terms of the gradient of the stress function and an auxiliary vector field, which is proved to verify a specifically defined anisotropic Laplace equation.

It is known that, for a 2D linear elastic anisotropic body, the stress field $\boldsymbol{\sigma} = \{\sigma_{xx}, \sigma_{yy}, \sigma_{xy}\}$

can be derived from a single stress function $\phi(\boldsymbol{x})$ [29]. By choosing

$$\sigma_{xx} = \phi_{,yy}, \quad \sigma_{yy} = \phi_{,xx}, \quad \sigma_{xy} = -\phi_{,xy} \tag{2}$$

the equilibrium equations are identically fulfilled. By using Eqs.(2), the two-dimensional elastic anisotropic constitutive law can be written as follows

$$\varepsilon_{xx} = s_{11}\phi_{,yy} + s_{12}\phi_{,xx} - s_{16}\phi_{,xy} \tag{3a}$$

$$\varepsilon_{yy} = s_{12}\phi_{,yy} + s_{22}\phi_{,xx} - s_{26}\phi_{,xy} \tag{3b}$$

$$\varepsilon_{xy} = s_{16}\phi_{,yy} + s_{26}\phi_{,xx} - s_{66}\phi_{,xy} \tag{3c}$$

where ε_{xx}, ε_{yy} and ε_{xy} denote the engineering strain components and the s_{11}, s_{22}, s_{66}, s_{12}, s_{16} and s_{66} are the compliance coefficients of a generic elastic anisotropic body. Equivalently, using the strain-displacement relations, one can write

$$u_{x,x} = s_{11}\phi_{,yy} + s_{12}\phi_{,xx} - s_{16}\phi_{,xy} \tag{4a}$$

$$u_{y,y} = s_{12}\phi_{,yy} + s_{22}\phi_{,xx} - s_{26}\phi_{,xy} \tag{4b}$$

$$u_{x,y} + u_{y,x} = s_{16}\phi_{,yy} + s_{26}\phi_{,xx} - s_{66}\phi_{,xy}. \tag{4c}$$

In Eqs.(2-3) and in the subsequent sections the comma used as a subscript denotes derivatives with respect to the coordinates identified by the subscripts following the comma itself.

Let us then consider the following vector field $\boldsymbol{v} = \{v_x, v_y\}$ chosen to satisfy the following relations

$$v_{x,x} = \kappa_1\phi_{,xx} + \phi_{,yy} + \kappa_3\phi_{,xy} \tag{5a}$$

$$v_{y,y} = \lambda_1\phi_{,xx} + \phi_{,yy} + \lambda_3\phi_{,xy} \tag{5b}$$

which allows to express $\phi_{,yy}$ and $\phi_{,xx}$ as follows

$$\phi_{,yy} = v_{x,x} - \kappa_1\phi_{,xx} - \kappa_3\phi_{,xy} \tag{6a}$$

$$\phi_{,xx} = \frac{1}{\lambda_1}v_{y,y} - \frac{1}{\lambda_1}\phi_{,yy} - \frac{\lambda_3}{\lambda_1}\phi_{,xy}. \tag{6b}$$

Upon substituting Eqs.(6a) and (6b) into Eqs.(4a) and (4b) respectively and integrating, it is possible to write the displacement $\boldsymbol{u}$ in terms of the vector field $\boldsymbol{v}$ and the gradient of the stress function ϕ, i.e.

$$u_x = s_{11}v_x + (s_{12} - s_{11}\kappa_1)\phi_{,x} - (s_{16} + s_{11}\kappa_3)\phi_{,y} \tag{7a}$$

$$u_y = s_{22}\frac{1}{\lambda_1}v_y - \left(s_{26} + s_{22}\frac{\lambda_3}{\lambda_1}\right)\phi_{,x} + \left(s_{12} - s_{22}\frac{1}{\lambda_1}\right)\phi_{,y} \tag{7b}$$

where the coefficients κ_1, κ_3, λ_1 and λ_3 will be obtained in the sequel. Eventually, taking the derivative of Eq.(7a) with respect to y and the derivative of Eq.(7b) with respect to x, and substituting into Eq.(4c), the following identity is obtained

$$\begin{aligned} s_{11}v_{x,y} + s_{22}\frac{1}{\lambda_1}v_{y,x} = &\left(2s_{26} + s_{22}\frac{\lambda_3}{\lambda_1}\right)\phi_{,xx} + (2s_{16} + s_{11}\kappa_3)\,\phi_{,yy} - \\ &\left(2s_{12} + s_{66} - s_{11}\kappa_1 - s_{22}\frac{1}{\lambda_1}\right)\phi_{,xy}. \end{aligned} \tag{8}$$

Let us now suppose that the components of the vector field $\boldsymbol{v}$, namely the functions v_x and v_y, satisfy the following anisotropic Laplace equation

$$v_{i,xx} + \square_1 v_{i,yy} + 2\square_2 v_{i,xy} = 0 \tag{9}$$

where $i = x, y$ and the coefficients $\square_1$ and $\square_2$ are in general different for v_x and v_y. The expressions of the derivative $v_{i,xx}$, $v_{i,yy}$ and $v_{i,xy}$ are obtained as follows: $v_{x,xx}$ and $v_{x,xy}$ are obtained upon taking the derivative of Eq.(5a) with respect to x and y, respectively; similarly, $v_{y,xy}$ and $v_{y,yy}$ are obtained upon taking the derivative of Eq.(5b) with respect to x and y, respectively; finally, $v_{x,yy}$ and $v_{y,xx}$ are obtained from Eq.(8) upon taking the derivative with respect to y and x, respectively. Let us consider v_x first.

Let v_x satisfy the following Laplace anisotropic equation

$$v_{x,xx} + a_1 v_{x,yy} + 2a_2 v_{x,xy} = 0. \tag{10}$$

Upon substituting the expressions of $v_{x,xx}$, $v_{x,xy}$ $v_{x,yy}$ from Eqs.(5a) and (8) into Eq.(10), one obtains

$$A_{xxx}\phi_{,xxx} + A_{xxy}\phi_{,xxy} + A_{xyy}\phi_{,xyy} + A_{yyy}\phi_{,yyy} = 0, \tag{11}$$

where

$$A_{xxx} = \kappa_1 - \frac{s_{22}}{s_{11}} a_1 \tag{12a}$$

$$A_{xxy} = 2a_2\kappa_1 + \kappa_3 + 2\frac{s_{26}}{s_{11}} a_1 \tag{12b}$$

$$A_{xyy} = 1 - a_1 \frac{2s_{12} + s_{66}}{s_{11}} + a_1\kappa_1 + 2a_2\kappa_3 \tag{12c}$$

$$A_{yyy} = 2a_2 + 2\frac{s_{16}}{s_{11}} a_1 + a_1\kappa_3. \tag{12d}$$

Eq.(11) is identically equal to zero if the coefficients A_{xxx}, A_{xxy}, A_{xyy} and A_{yyy} are identically zero. Upon forcing Eqs.(12a-d) to be zero, it is therefore possible to obtain the expression for the coefficients κ_1, κ_3, a_1 and a_2. It is interesting to note that in Eqs.(12a-d) the coefficients λ_1 and λ_3 do not appear.

Similarly, let v_y satisfy the following Laplace anisotropic equation

$$v_{y,xx} + b_1 v_{y,yy} + 2b_2 v_{y,xy} = 0. \tag{13}$$

Using the expressions of $v_{y,xx}$, $v_{y,xy}$ $v_{y,yy}$ from Eqs.(5b) and (8) into Eq.(13), one has

$$B_{xxx}\phi_{,xxx} + B_{xxy}\phi_{,xxy} + B_{xyy}\phi_{,xyy} + B_{yyy}\phi_{,yyy} = 0, \tag{14}$$

where

$$B_{yyy} = b_1 - \frac{s_{11}}{s_{22}} \lambda_1 \tag{15a}$$

$$B_{xyy} = 2b_2 + b_1\lambda_3 + 2\frac{s_{16}}{s_{22}} \lambda_1 \tag{15b}$$

$$B_{xxy} = 1 - \lambda_1 \frac{2s_{12} + s_{66}}{s_{22}} + b_1\lambda_1 + 2b_2\lambda_3 \tag{15c}$$

$$B_{xxx} = 2b_2\lambda_1 + 2\frac{s_{16}}{s_{22}} \lambda_1 + \lambda_3. \tag{15d}$$

Eq.(14) is identically equal to zero if the coefficients B_{xxx}, B_{xxy}, B_{xyy} and B_{yyy} are identically zero. Upon forcing Eqs.(15a-d) to be zero, it is therefore possible to obtain the

coefficients λ_1, λ_3, b_1 and b_2. It is interesting to note that in Eqs.(15a-d) the coefficients κ_1 and κ_3 do not appear.

Eventually, it is interesting to note that Eqs.(15) are retrieved from Eqs.(12) if in Eqs.(12) the coefficients κ_1, κ_3, a_1 and a_2 are replaced with λ_1, λ_3, b_1 and b_2, respectively. In particular, it possible to notice that, after the aforementioned substitution, $B_{yyy} \equiv A_{xxx}$, $B_{xyy} \equiv A_{yyy}$, $B_{xxy} \equiv A_{xyy}$ and $B_{xxx} \equiv A_{xxy}$. Therefore, prior to obtaining the explicit expression of the coefficients, it is the possible to assert that: (i) $a_1 \equiv b_1$, $a_2 \equiv b_2$, $\kappa_1 \equiv \lambda_1$ and $\kappa_3 \equiv \lambda_3$; (ii) v_x and v_y satisfy the same anisotropic Laplace equation; (iii) the following conjugate relationships hold

$$v_{x,x} = v_{y,y} \tag{16a}$$

$$a_1 v_{x,y} + a_2 v_{y,y} = -(v_{y,x} + a_2 v_{x,x}). \tag{16b}$$

The explicit expression of the introduced coefficients is then obtained for the cases of isotropic, orthotropic and generally anisotropic materials.

3.1. Isotropic materials

In the isotropic case, i.e. $s_{11} = s_{22}$, $s_{16} = s_{26} = 0$ and $2s_{12} + s_{66} = 2s_{11}$, the following solution is obtained for the coefficients κ_1, κ_3, a_1 and a_2:

$$\kappa_1 = 1 \tag{17a}$$

$$\kappa_3 = 0 \tag{17b}$$

$$a_1 = 1 \tag{17c}$$

$$a_2 = 0. \tag{17d}$$

3.2. Orthotropic materials

In the orthotropic case, i.e. $s_{16} = s_{26} = 0$, the following solution is obtained for the coefficients κ_1, κ_3, a_1 and a_2:

$$\kappa_1 = a_1 s_{22}/s_{11} \tag{18a}$$

$$\kappa_3 = 0 \tag{18b}$$

$$a_2 = 0 \tag{18c}$$

and a_1 is one of the roots of the following sixth-order polynomial

$$[s_{22}a_1^2 - (2s_{12} + s_{66})a_1 + s_{11}](s_{22}a_1^2 - s_{11})^2 = 0. \tag{19}$$

3.3. Anisotropic materials

In the generally anisotropic case, a suitable manipulation of Eqs.(12a-d) leads to

$$\kappa_1 = a_1 s_{22}/s_{11} \tag{20a}$$

$$\kappa_3 = 2\frac{a_1(a_1 s_{16} s_{22} - s_{11} s_{26})}{s_{11}(s_{11} - a_1^2 s_{22})} \tag{20b}$$

$$a_2 = \frac{a_1(a_1 s_{26} - s_{16})}{s_{11} - s_{22}a_1^2} \tag{20c}$$

where a_1 is one of the roots of the following sixth-order polynomial

$$\Sigma_6 a_1^6 + \Sigma_5 a_1^5 + \Sigma_4 a_1^4 + \Sigma_3 a_1^3 + \Sigma_2 a_1^2 + \Sigma_1 a_1 + \Sigma_0 = 0 \tag{21}$$

being

$$\Sigma_6 = s_{22}^3 \tag{22a}$$

$$\Sigma_5 = -s_{22}^2(2s_{12} + s_{66}) \tag{22b}$$

$$\Sigma_4 = s_{22}(4s_{16}s_{26} - s_{11}s_{22}) \tag{22c}$$

$$\Sigma_3 = 4s_{11}s_{12}s_{22} - 4s_{16}^2 s_{22} - 4s_{26}^2 s_{11} + 2s_{11}s_{22}s_{66} \tag{22d}$$

$$\Sigma_2 = s_{11}(4s_{16}s_{26} - s_{11}s_{22}) \tag{22e}$$

$$\Sigma_1 = -s_{11}^2(2s_{12} + s_{66}) \tag{22f}$$

$$\Sigma_0 = s_{11}^3. \tag{22g}$$

3.4. Displacement decomposition in matricial form

Finally, as soon as the values of a_1, a_2, κ_1 and κ_3, and therefore of b_1, b_2, λ_1 and λ_3, are obtained, it is possible to write Eqs.(7a) and (7b) in matricial form as follows

$$\boldsymbol{u} = \boldsymbol{L}\boldsymbol{v} - \boldsymbol{\Lambda}\nabla\phi \tag{23}$$

where $\nabla\phi = \{\phi_{,x}, \phi_{,y}\}$ denotes the gradient of the stress function, and

$$\boldsymbol{L} = s_{11}\begin{bmatrix} 1 & 0 \\ 0 & \frac{1}{a_1} \end{bmatrix} \quad \text{and} \quad \boldsymbol{\Lambda} = \begin{bmatrix} s_{11}\lambda - s_{12} & s_{16} + s_{11}\kappa \\ s_{26} + s_{22}\frac{\kappa}{\lambda} & s_{22}\frac{1}{\lambda} - s_{12} \end{bmatrix} \tag{24}$$

being $\lambda = \lambda_1 = \kappa_1$ and $\kappa = \lambda_3 = \kappa_3$. Eq.(23) denotes the displacement decomposition that will be used to derive an additional integral equation for anisotropic elasticity as shown in the following section.

4. Alternative displacement boundary integral equation

The starting point for the proposed derivation is the integral representation of the components of the vector field $\boldsymbol{v}$, v_x and v_y, which satisfy the anisotropic Laplace equation (10) or (13). Since v_x and v_y verify the *same* Laplace equation, it is easy to show that the vector field $\boldsymbol{v}$ verify the following integral equation

$$c(\boldsymbol{x}_0)\boldsymbol{v}(\boldsymbol{x}_0) + \fint_S p^*(\boldsymbol{x}, \boldsymbol{x}_0)\boldsymbol{v}(\boldsymbol{x})\mathrm{d}S(\boldsymbol{x}) = \int_S v^*(\boldsymbol{x}, \boldsymbol{x}_0)\boldsymbol{p}(\boldsymbol{x})\mathrm{d}S(\boldsymbol{x}), \tag{25}$$

where $c(\boldsymbol{x}_0)$ denotes the free term and $\boldsymbol{p}(\boldsymbol{x})$ represents the flux of $\boldsymbol{v}(\boldsymbol{x})$, which is given by

$$\boldsymbol{p}(\boldsymbol{x}) = \frac{\partial \boldsymbol{v}}{\partial \widetilde{n}}(\boldsymbol{x}) \equiv [\boldsymbol{v}_{,x}(\boldsymbol{x}) + a_2\boldsymbol{v}_{,y}(\boldsymbol{x})]n_x(\boldsymbol{x}) + [a_2\boldsymbol{v}_{,x}(\boldsymbol{x}) + a_1\boldsymbol{v}_{,y}(\boldsymbol{x})]n_y(\boldsymbol{x}) \tag{26}$$

being $\boldsymbol{n} = \{n_x, n_y\}$ the normal unit vector of the boundary S at the point $\boldsymbol{x}$. In Eq.(25), $v^*(\boldsymbol{x}, \boldsymbol{x}_0)$ and $p^*(\boldsymbol{x}, \boldsymbol{x}_0)$ are the kernels of the integral equation and their expression is given as follows:

$$v^*(\boldsymbol{x}, \boldsymbol{x}_0) = -\frac{1}{2\pi\sqrt{a_1 - a_2^2}}\ln\widetilde{r} \tag{27a}$$

and

$$p^*(\boldsymbol{x},\boldsymbol{x}_0) = \frac{\partial v^*}{\partial \widetilde{n}}(\boldsymbol{x},\boldsymbol{x}_0), \tag{27b}$$

where $\widetilde{r} = \sqrt{r_x^2 + 2(a_2/a_1)r_x r_y + r_y^2/a_1}$ being $r_x = x - x_0$ and $r_y = y - y_0$.

It is interesting to note that if $\boldsymbol{s} = \{s_x, s_y\} = \{-n_y, n_x\}$ denotes the unit vector tangent to S at $\boldsymbol{x}$, and if we consider the conjugate relationships expressed in Eqs.(16), the following identity holds for the vector field $\boldsymbol{v}$

$$\frac{\partial \boldsymbol{v}}{\partial \widetilde{n}} = \boldsymbol{A}\frac{\partial \boldsymbol{v}}{\partial s} \quad \text{with} \quad \boldsymbol{A} = \begin{bmatrix} a_2 & 1 \\ -a_1 & -a_2 \end{bmatrix}. \tag{28}$$

It is also noted that the boundary tractions $\boldsymbol{t}$ can be expressed in terms of the gradient of the stress function ϕ, i.e.

$$\boldsymbol{t} = \boldsymbol{\Psi}\frac{\partial \nabla\phi}{\partial s}, \quad \text{with} \quad \boldsymbol{\Psi} = \begin{bmatrix} 0 & 1 \\ -1 & 0 \end{bmatrix} \tag{29}$$

It is now possible to transform Eq.(25) into an integral equation involving boundary displacements and tractions only. More specifically, substituting Eqs.(23), (28) and (29) into Eq.(25), one obtains the following integral equation

$$\begin{aligned} c(\boldsymbol{x}_0)\boldsymbol{u}(\boldsymbol{x}_0) + c(\boldsymbol{x}_0)\boldsymbol{\Lambda}\nabla\phi(\boldsymbol{x}_0) + \fint_S \boldsymbol{P}(\boldsymbol{x},\boldsymbol{x}_0)\boldsymbol{u}(\boldsymbol{x})\mathrm{d}S(\boldsymbol{x}) + \\ + \fint_S \boldsymbol{P}^*_\phi(\boldsymbol{x},\boldsymbol{x}_0)\nabla\phi(\boldsymbol{x})\mathrm{d}S(\boldsymbol{x}) = \int_S \boldsymbol{V}(\boldsymbol{x},\boldsymbol{x}_0)\boldsymbol{t}(\boldsymbol{x})\mathrm{d}S(\boldsymbol{x}), \end{aligned} \tag{30}$$

where the following kernels have been introduced

$$\boldsymbol{V}(\boldsymbol{x},\boldsymbol{x}_0) = \boldsymbol{L}\boldsymbol{A}\boldsymbol{L}^{-1}\boldsymbol{\Lambda}\boldsymbol{\Psi}^{-1}v^*(\boldsymbol{x},\boldsymbol{x}_0), \tag{31a}$$

$$\boldsymbol{P}(\boldsymbol{x},\boldsymbol{x}_0) = \boldsymbol{I}p^*(\boldsymbol{x},\boldsymbol{x}_0) + \boldsymbol{L}\boldsymbol{A}\boldsymbol{L}^{-1}\frac{\partial v^*}{\partial s}(\boldsymbol{x},\boldsymbol{x}_0), \tag{31b}$$

$$\boldsymbol{P}^*_\phi(\boldsymbol{x},\boldsymbol{x}_0) = \boldsymbol{\Lambda}p^*(\boldsymbol{x},\boldsymbol{x}_0). \tag{31c}$$

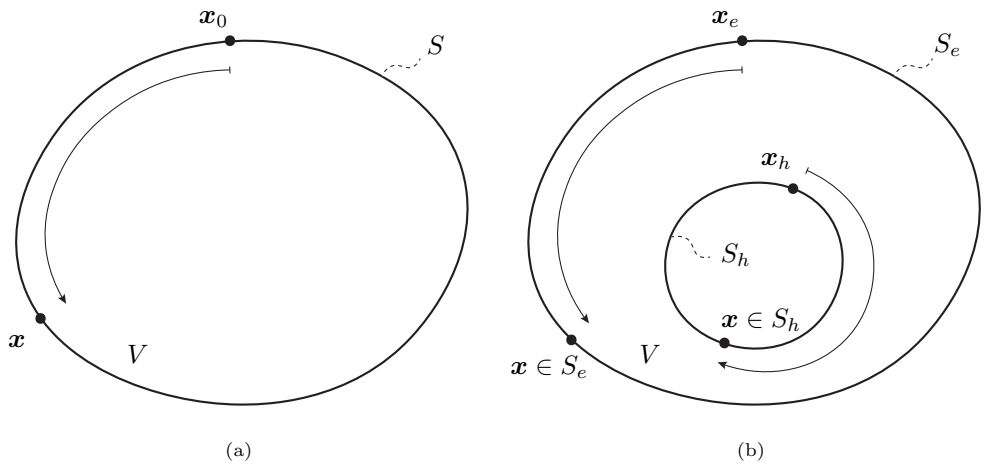

Figure 1: Example of a (a) simply- and a (b) doubly-connected domain. The arrows denotes the paths along which the tractions resultants are computed.

Eq.(30) can be seen as a boundary integral representation of the stress function gradient. The sought alternative displacement boundary integral equation is obtained in the subsequent sections. However, as shown next, it is necessary to distinguish between the cases of simply- and multiply-connected domains.

4.1. Simply-connected domains

In simply-connected domains, it is always possible to define a curve going from a point $\boldsymbol{x}_0$ on the boundary S to another point $\boldsymbol{x} \in S$, as sketched in Fig.(1a). Along such a path, it is possible to define the resultant $\boldsymbol{R}$ of the tractions $\boldsymbol{t}$ as

$$\boldsymbol{R}(\boldsymbol{x}, \boldsymbol{x}_0) = \int_{\boldsymbol{x}_0}^{\boldsymbol{x}} \boldsymbol{t}(\widetilde{\boldsymbol{x}}) \mathrm{d}S(\widetilde{\boldsymbol{x}}), \tag{32}$$

whereby, upon integration of Eq.(29), one obtains

$$\boldsymbol{R}(\boldsymbol{x}, \boldsymbol{x}_0) = \boldsymbol{\Psi}[\nabla\phi(\boldsymbol{x}) - \nabla\phi(\boldsymbol{x}_0)]. \tag{33}$$

Substituting Eq.(33) into Eq.(30), one obtains the sought alternative displacement boundary integral equation for simply-connected domains as follows

$$c(\boldsymbol{x}_0)\boldsymbol{u}(\boldsymbol{x}_0) + \fint_S \boldsymbol{P}(\boldsymbol{x},\boldsymbol{x}_0)\boldsymbol{u}(\boldsymbol{x})\mathrm{d}S(\boldsymbol{x}) = \\ = \int_S \boldsymbol{V}(\boldsymbol{x},\boldsymbol{x}_0)\boldsymbol{t}(\boldsymbol{x})\mathrm{d}S(\boldsymbol{x}) - \fint_S \boldsymbol{P}_\phi(\boldsymbol{x},\boldsymbol{x}_0)\boldsymbol{R}(\boldsymbol{x},\boldsymbol{x}_0)\mathrm{d}S(\boldsymbol{x}) \quad (34)$$

where the kernel $\boldsymbol{P}_\phi(\boldsymbol{x},\boldsymbol{x}_0) = \boldsymbol{P}^*_\phi(\boldsymbol{x},\boldsymbol{x}_0)\boldsymbol{\Psi}^{-1}$ has been introduced and the identity $c(\boldsymbol{x}_0) = -\fint_S p^*(\boldsymbol{x},\boldsymbol{x}_0)\mathrm{d}S(\boldsymbol{x})$ has been used.

4.2. Multiply-connected domains

Without loss of generality, let us consider a doubly-connected domain as shown in Fig.(1b). The domain V is supposed to have an external boundary S^e and an internal hole bounded by S^h. For such a domain it is possible to write Eq.(25) or Eq.(30) considering that the boundary S consists of the external boundary and the hole boundary, i.e. $S = S^e \cup S^h$. However, in this case it is not possible to integrate the tractions from a point $\boldsymbol{x}_h \in S^h$ to another point $\boldsymbol{x} \in S^e$ without going through the domain. Therefore, different tractions resultants must be defined for the external boundary and for the hole, which leads to the following expressions:

$$\boldsymbol{R}(\boldsymbol{x},\boldsymbol{x}_e) = \boldsymbol{\Psi}[\nabla\phi(\boldsymbol{x}) - \nabla\phi(\boldsymbol{x}_e)], \quad \boldsymbol{x},\boldsymbol{x}_e \in S^e, \quad (35a)$$

$$\boldsymbol{R}(\boldsymbol{x},\boldsymbol{x}_h) = \boldsymbol{\Psi}[\nabla\phi(\boldsymbol{x}) - \nabla\phi(\boldsymbol{x}_h)], \quad \boldsymbol{x},\boldsymbol{x}_h \in S^h. \quad (35b)$$

It follows that collocating at $\boldsymbol{x}_e \in S^e$ and using Eqs.(35), Eq.(30) becomes

$$c(\boldsymbol{x}_e)\boldsymbol{u}(\boldsymbol{x}_e) + \fint_{S^e} \boldsymbol{P}(\boldsymbol{x},\boldsymbol{x}_e)\boldsymbol{u}(\boldsymbol{x})\mathrm{d}S(\boldsymbol{x}) + \int_{S^h} \boldsymbol{P}(\boldsymbol{x},\boldsymbol{x}_e)\boldsymbol{u}(\boldsymbol{x})\mathrm{d}S(\boldsymbol{x}) = \\ = \int_{S^e\cup S^h} \boldsymbol{V}(\boldsymbol{x},\boldsymbol{x}_e)\boldsymbol{t}(\boldsymbol{x})\mathrm{d}S(\boldsymbol{x}) - \int_{S^e} \boldsymbol{P}_\phi(\boldsymbol{x},\boldsymbol{x}_e)\boldsymbol{R}(\boldsymbol{x},\boldsymbol{x}_e)\mathrm{d}S(\boldsymbol{x}) - \\ \int_{S^h} \boldsymbol{P}_\phi(\boldsymbol{x},\boldsymbol{x}_e)\boldsymbol{R}(\boldsymbol{x},\boldsymbol{x}_h)\mathrm{d}S(\boldsymbol{x}) \quad (36)$$

whereas, collocating at $\boldsymbol{x}_h \in S^h$ leads to

$$
\begin{aligned}
c(\boldsymbol{x}_h)\boldsymbol{u}(\boldsymbol{x}_h) + \fint_{S^e \cup S^h} \boldsymbol{P}(\boldsymbol{x}, \boldsymbol{x}_h)\boldsymbol{u}(\boldsymbol{x})\mathrm{d}S(\boldsymbol{x}) + \boldsymbol{\Lambda}(\nabla\phi(\boldsymbol{x}_h) - \nabla\phi(\boldsymbol{x}_e)) = \\
= \int_{S^e \cup S^h} \boldsymbol{V}(\boldsymbol{x}, \boldsymbol{x}_h)\boldsymbol{t}(\boldsymbol{x})\mathrm{d}S(\boldsymbol{x}) - \int_{S^e} \boldsymbol{P}_\phi(\boldsymbol{x}, \boldsymbol{x}_h)\boldsymbol{R}(\boldsymbol{x}, \boldsymbol{x}_e)\mathrm{d}S(\boldsymbol{x}) - \\
\int_{S^h} \boldsymbol{P}_\phi(\boldsymbol{x}, \boldsymbol{x}_h)\boldsymbol{R}(\boldsymbol{x}, \boldsymbol{x}_h)\mathrm{d}S(\boldsymbol{x}).
\end{aligned} \tag{37}
$$

Eqs.(36) and (37) represent the sought alternative displacement boundary integral equation for multiply-connected domains when collocation is performed on the external boundary or on the internal hole, respectively.

It is worth noting that Eqs.(37) contains the difference between the values of the stress function gradient at the points $\boldsymbol{x}_h$ and $\boldsymbol{x}_e$. The presence of this additional constant is consistent with the fact that it is not possible to find the solution of a multiply connected domain in terms of a stress function without introducing additional conditions. The technique to eliminate such a constant will be discussed in Section (7).

5. Application to fracture mechanics

Once the boundary integral equations (34) and (37) have been introduced, they can be used in combination with Eq.(1) to solve the fracture mechanics problem via a single-region approach.

The collocation of Eq.(1) at $\boldsymbol{x}_0^+ \in C$ leads to the following integral equation:

$$
\begin{aligned}
\boldsymbol{c}(\boldsymbol{x}_0^+)\boldsymbol{u}(\boldsymbol{x}_0^+) + \boldsymbol{c}(\boldsymbol{x}_0^-)\boldsymbol{u}(\boldsymbol{x}_0^-) + \fint_S \boldsymbol{T}(\boldsymbol{x}, \boldsymbol{x}_0^+)\boldsymbol{u}(\boldsymbol{x})\mathrm{d}S(\boldsymbol{x}) + \\
+ \fint_C \boldsymbol{T}(\boldsymbol{x}, \boldsymbol{x}_0^+)\delta\boldsymbol{u}(\boldsymbol{x})\mathrm{d}S(\boldsymbol{x}) = \int_S \boldsymbol{U}(\boldsymbol{x}, \boldsymbol{x}_0^+)\boldsymbol{t}(\boldsymbol{x})\mathrm{d}S(\boldsymbol{x}).
\end{aligned} \tag{38}
$$

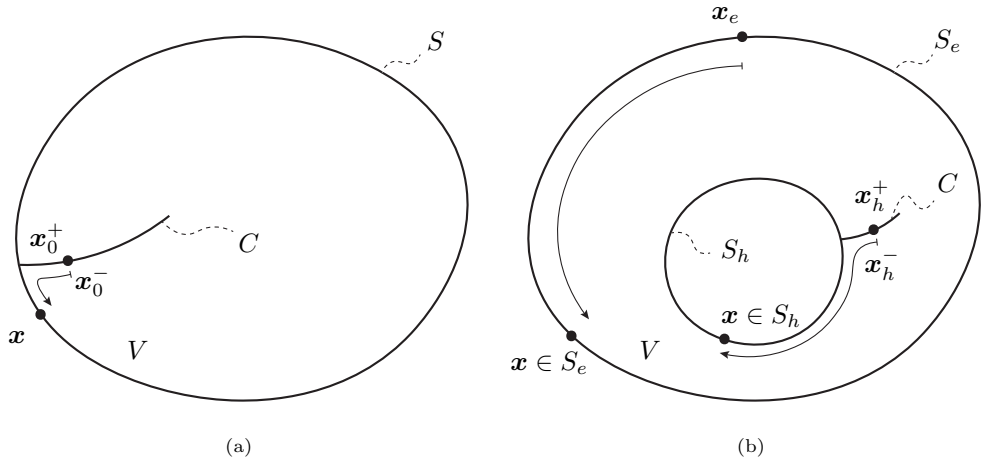

Figure 2: Example of a cracked (a) simply- and (b) doubly-connected domain. The arrows denotes the paths along which the tractions resultants are computed.

It is worth noting that such an equation is valid for both simply-connected and multiply-connected domains provided that the boundary S appearing in Eq.(38) denotes the union of the external and the internal boundaries.

On the other hand, Eq.(34) or (37) must be suitably selected on the basis of the location of crack within the domain. Considering a cracked simply-connected domain as the one shown in Fig.(2a), it is always possible to define the tractions resultant between two points of the boundary S. In fact, collocating Eq.(34) at $\boldsymbol{x}_0^- \in C$ and assuming that the crack is traction-free, one obtains

$$c(\boldsymbol{x}_0^-)\boldsymbol{u}(\boldsymbol{x}_0^-) + c(\boldsymbol{x}_0^+)\boldsymbol{u}(\boldsymbol{x}_0^+) + \fint_S \boldsymbol{P}(\boldsymbol{x}, \boldsymbol{x}_0^-)\boldsymbol{u}(\boldsymbol{x})\mathrm{d}S(\boldsymbol{x}) + \fint_C \boldsymbol{P}(\boldsymbol{x}, \boldsymbol{x}_0^-)\delta\boldsymbol{u}(\boldsymbol{x})\mathrm{d}S(\boldsymbol{x}) = \int_S \boldsymbol{V}(\boldsymbol{x}, \boldsymbol{x}_0^-)\boldsymbol{t}(\boldsymbol{x})\mathrm{d}S(\boldsymbol{x}) - \fint_S \boldsymbol{P}_\phi(\boldsymbol{x}, \boldsymbol{x}_0^-)\boldsymbol{R}(\boldsymbol{x}, \boldsymbol{x}_0^-)\mathrm{d}S(\boldsymbol{x}). \tag{39}$$

Finally, referring to the cracked doubly-connected domain shown in Fig.(2b), different boundary paths must be considered to define the tractions resultants. Analogously to the derivation of Eq.(37), collocating at $\boldsymbol{x}_h^- \in C$ of the domain shown in Fig.(2b) and

assuming that the crack C is traction-free, one obtains the following equation:

$$
\begin{aligned}
c(\boldsymbol{x}_h^+)\boldsymbol{u}(\boldsymbol{x}_h^+)+c(\boldsymbol{x}_h^-)\boldsymbol{u}(\boldsymbol{x}_h^-) + \int_{S^e\cup S^h} \boldsymbol{P}(\boldsymbol{x},\boldsymbol{x}_h^-)\boldsymbol{u}(\boldsymbol{x})\mathrm{d}S(\boldsymbol{x})+ \\
\fint_C \boldsymbol{P}(\boldsymbol{x},\boldsymbol{x}_h^-)\delta\boldsymbol{u}(\boldsymbol{x})\mathrm{d}S(\boldsymbol{x}) + \boldsymbol{\Lambda}(\nabla\phi(\boldsymbol{x}_h^-) - \nabla\phi(\boldsymbol{x}_e)) = \\
\int_{S^e\cup S^h} \boldsymbol{V}(\boldsymbol{x},\boldsymbol{x}_h^-)\boldsymbol{t}(\boldsymbol{x})\mathrm{d}S(\boldsymbol{x}) - \int_{S^e} \boldsymbol{P}_\phi(\boldsymbol{x},\boldsymbol{x}_h^-)\boldsymbol{R}(\boldsymbol{x},\boldsymbol{x}_e)\mathrm{d}S(\boldsymbol{x}) - \\
\int_{S^h} \boldsymbol{P}_\phi(\boldsymbol{x},\boldsymbol{x}_h^-)\boldsymbol{R}(\boldsymbol{x},\boldsymbol{x}_h^-)\mathrm{d}S(\boldsymbol{x}).
\end{aligned}
\tag{40}
$$

6. Discretization

The numerical discretisation of the alternative integral equations derived in the previous sections follows the same approach as that used in the discretisation of the displacement boundary integral equation (1), which can be found in many textbooks on the Boundary Element Method [4, 5]. The only boundary integrals that deserve particular attention are those related to the evaluation of the tractions resultants.

Let us consider two points $\boldsymbol{x}_0$ and $\boldsymbol{x}$ belonging to the same boundary S, which is divided into N_e non-overlapping mesh elements. Let us also assume x_0 is contained within the m_0-th element and x is contained within the m-element as shown in Fig.(3). The tractions resultant $\boldsymbol{R}(\boldsymbol{x}_0,\boldsymbol{x})$ can then be written as the sum of the contributions of each element between $\boldsymbol{x}_0$ and $\boldsymbol{x}$, i.e.

$$
\boldsymbol{R}(\boldsymbol{x},\boldsymbol{x}_0) = \int_{\boldsymbol{x}_0}^{\boldsymbol{b}_{m_0}} \boldsymbol{t}(\widetilde{\boldsymbol{x}})\mathrm{d}S(\widetilde{\boldsymbol{x}}) + \sum_{\epsilon=m_0+1}^{m-1} \int_{\epsilon} \boldsymbol{t}(\widetilde{\boldsymbol{x}})\mathrm{d}S(\widetilde{\boldsymbol{x}}) + \int_{\boldsymbol{a}_m}^{\boldsymbol{x}} \boldsymbol{t}(\widetilde{\boldsymbol{x}})\mathrm{d}S(\widetilde{\boldsymbol{x}}) \tag{41}
$$

where $\boldsymbol{b}_{m_0}$ is the end point of element m_0, $\epsilon = m_0+1,\ldots,m-1$ identifies the elements of S that one needs to travel to go from $\boldsymbol{b}_{m_0}$ to $\boldsymbol{a}_m$, and $\boldsymbol{a}_m$ is the start point of the

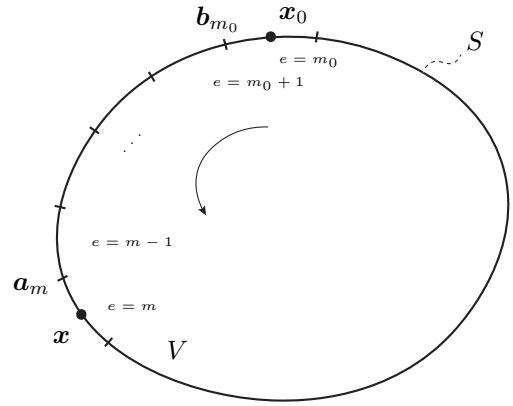

Figure 3: Scheme for the discretization of the traction resultants.

element m. Using a local variable ξ to map the geometry and the primary variables, namely displacements and tractions, of the boundary elements, one has

$$\boldsymbol{x}(\xi) = \sum_{\beta=1}^{\mu} \mathcal{M}^{\beta}(\xi)\boldsymbol{x}^{\epsilon\beta} \tag{42a}$$

and

$$\boldsymbol{u}[\boldsymbol{x}(\xi)] = \sum_{\alpha=1}^{\nu} \mathcal{N}^{\alpha}(\xi)\boldsymbol{u}^{\epsilon\alpha}, \quad \boldsymbol{t}[\boldsymbol{x}(\xi)] = \sum_{\alpha=1}^{\nu} \mathcal{N}^{\alpha}(\xi)\boldsymbol{t}^{\epsilon\alpha}, \tag{42b}$$

where: $\mathcal{M}^{\beta}(\xi)$ and $\mathcal{N}^{\alpha}(\xi)$ are the shape functions approximating the geometry of the boundary and the unknown boundary fields, respectively; $\boldsymbol{x}^{\epsilon\beta}$ are the coordinates of the points used to approximate the ϵ-th boundary element; $\boldsymbol{u}^{\epsilon\alpha}$ and $\boldsymbol{t}^{\epsilon\alpha}$ the nodal values of displacements and tractions, respectively; μ and ν are the number of geometrical points and the number of the degrees of freedom of the element, respectively; and $J^{\epsilon}(\xi) \equiv |\mathrm{d}\boldsymbol{x}(\xi)/\mathrm{d}\xi|$ denotes the Jacobian of the map $\boldsymbol{x} = \boldsymbol{x}(\xi)$ for the ϵ-th boundary element.

Using the approximation introduced with Eqs.(42a) and (42b), the discretized version

of the tractions resultant in Eq.(41) can be written

$$\boldsymbol{R}(\boldsymbol{x},\boldsymbol{x}_0) = \sum_{\alpha=1}^{\nu}\left(\int_{\xi_0}^{1}\mathcal{N}^{\alpha}(\xi)J^{m_0}(\xi)\mathrm{d}\xi\right)\boldsymbol{t}^{m_0\alpha}+ \\ \sum_{\epsilon=m_0+1}^{m-1}\sum_{\alpha=1}^{\nu}\left(\int_{-1}^{+1}\mathcal{N}^{\alpha}(\xi)J^{\epsilon}(\xi)\mathrm{d}\xi\right)\boldsymbol{t}^{\epsilon\alpha}+\sum_{\alpha=1}^{\nu}\left(\int_{-1}^{\xi}\mathcal{N}^{\alpha}(\widetilde{\xi})J^{n}(\widetilde{\xi})\mathrm{d}\widetilde{\xi}\right)\boldsymbol{t}^{m\alpha} = \\ \sum_{\alpha=1}^{\nu}\Theta^{m_0\alpha}(\xi_0,1)\boldsymbol{t}^{m_0\alpha}+\sum_{\epsilon=m_0+1}^{m-1}\sum_{\alpha=1}^{\nu}\Theta^{\epsilon\alpha}(-1,1)\boldsymbol{t}^{\epsilon\alpha}+\sum_{\alpha=1}^{\nu}\Theta^{m\alpha}(-1,\xi)\boldsymbol{t}^{m\alpha} \tag{43}$$

where

$$\Theta^{\epsilon\alpha}(a,b) \equiv \int_a^b \mathcal{N}^{\alpha}(\xi)J^{\epsilon}(\xi)\mathrm{d}\xi \tag{44}$$

and ξ_0 is the value of the local variable ξ on the element containing $\boldsymbol{x}_0$ at which $\boldsymbol{x}(\xi_0) = \boldsymbol{x}_0$. Eq.(43) shows that the tractions resultants are written in terms of the tractions degrees of freedom. Therefore, the discrete version of the alternative integral equations introduced in the previous sections can be written in the form $\boldsymbol{HU} = \boldsymbol{GT}$ as classically done for the displacement boundary integral equations [5].

7. Numerical results

7.1. Notched and cracked domain solution

The derived alternative equation is first employed to model the elastic response of both notched and cracked domains. The results are presented for different domains assuming isotropic as well as generally anisotropic behavior.

For the isotropic case the material properties has been set as $E = 1.0$GPa and $\nu = 0.3$ being E the Young's modulus and ν the Poisson's ratio. The stiffness matrix used for the

anisotropic case reads as

$$\boldsymbol{C} = \begin{bmatrix} 0.5637 & 0.2963 & 0.3158 \\ 0.2963 & 0.5637 & 0.3158 \\ 0.3158 & 0.3158 & 0.3111 \end{bmatrix} \text{ GPa} \tag{45}$$

and corresponds to the in-plane behaviour of a [30/60/60/30] symmetric laminate with 2.5 mm thick orthotropic plies having $E_1 = 15.5\,\text{GPa}$, $E_2 = 1.0\,\text{GPa}$; $G_{12} = 0.45\,\text{GPa}$ and $\nu_{12} = 0.3$. It is worth noting that these constants characterize a non-degenerate anisotropic material and thus the expressions of the fundamental solution given in [5] can be used in computations.

Numerical tests are performed using quadratic elements with the semi-discontinuous option to deal with corners. Tractions boundary conditions are considered and the technique proposed by Lutz et al.[30] is used to avoid the rigid body degrees of freedom. The obtained results are compared with a reference solution, which for uncracked domains is obtained using Eq.(1) only, whereas, for cracked domains is computed using Eq.(1) and a multi-region approach.

Figures (4a) and (4b) shows the geometry and the mesh, respectively, of a notched square domain. The domain is loaded by uniform tractions over the top and bottom edges whereas the remaining boundaries are kept traction-free. The analysis has been carried out by collocating Eq.(34) over the notch of the domain as sketched in Fig.(4a), and Eq.(1) on the remaining boundaries. The accuracy of the proposed formulation is then shown in Figs.(5a) and (5b), which report the comparison between the results obtained and the

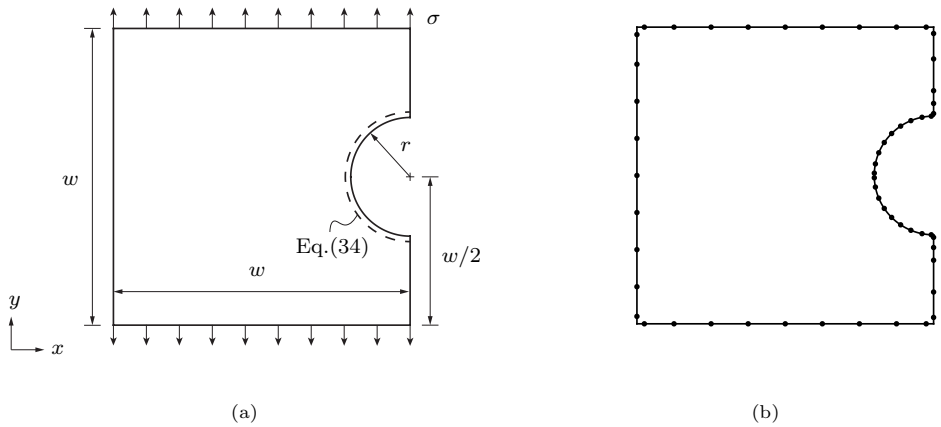

Figure 4: Notched square domain: (a) Geometry and loads: $r = w/5$; (b) Mesh.

reference solution for the cases of isotropic and anisotropic behaviour, respectively. In the following figures the results of the reference solutions are depicted as black dashed line whereas red continuous line is used for the present approach results.

The second test involves a square domain with an internal hole, i.e. a doubly-connected domain. The domain is shown in Fig.(6a) and is loaded by uniform tractions over the top and bottom edges, whereas the remaining boundaries, including the internal hole, are kept traction-free. The employed mesh of the domain is shown in Fig.(6b).

In this case, the analysis is performed by collocating Eq.(37) over one half of the internal hole and Eq.(1) on the remaining boundaries, see Fig.(6a). Moreover, it is worth recalling that Eq.(37) contains an additional unknown constant, namely the term $\boldsymbol{\Lambda}(\nabla\phi(\boldsymbol{x}_h)-\nabla\phi(\boldsymbol{x}_e))$. To eliminate such a constant, Eq.(37) is collocated at one additional point of the hole's boundary and subtracted from all the other equations stemming from

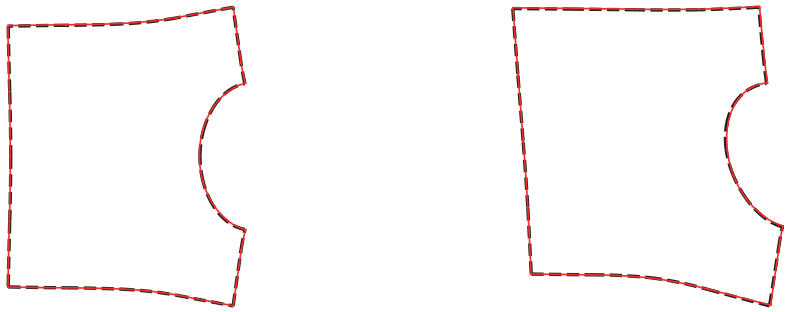

(a) (b)

Figure 5: Deformed shape of the notched square domain: (a) isotropic and (b) anisotropic.

the collocation of Eq.(37). The obtained results are shown in Figs.(7a) and (7b) in the cases of isotropic and anisotropic behaviour, respectively, and demonstrate the accuracy of the proposed formulation.

The third test involves a square domain with an edge crack. The domain is shown in Fig.(8a) and is loaded by uniform tractions over the top and bottom edges, whereas the remaining boundaries, including the crack lines, are kept traction-free. It is worth recalling that in such a case of the edge crack, the domain can be considered as simply connected, thus allowing for the use of Eq.(39). The employed mesh of the domain is shown in Fig.(8b) where it is possible to notice that the crack tip is modelled as continuous.

For this case, the reference solution is obtained via the multi-region approach. More specifically, the domain is divided into two subdomains by introducing a fictitious boundary that connects the crack tip and an arbitrary point of the domain; along such an

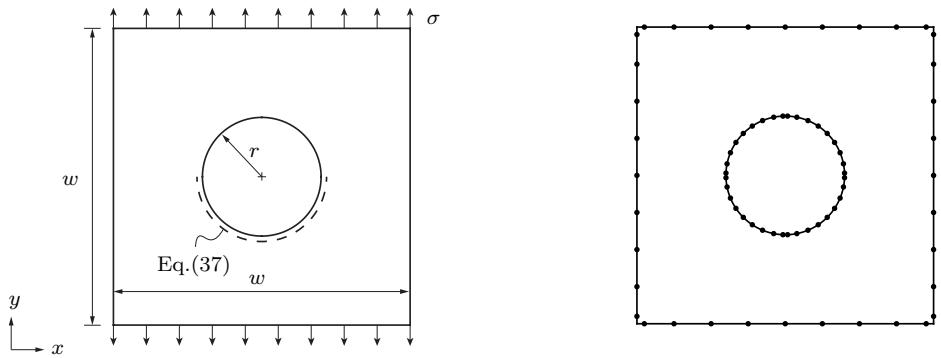

(a) (b)

Figure 6: Square domain with a centered internal hole: (a) Geometry and loads: $r = w/5$; (b) Mesh.

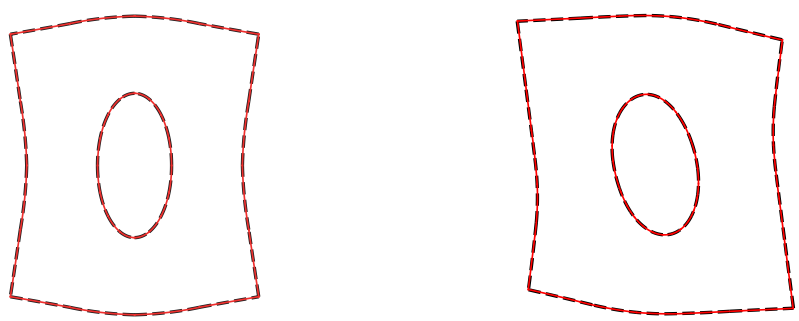

(a) (b)

Figure 7: Deformed shape of the square domain with an internal hole: (a) isotropic and (b) anisotropic.

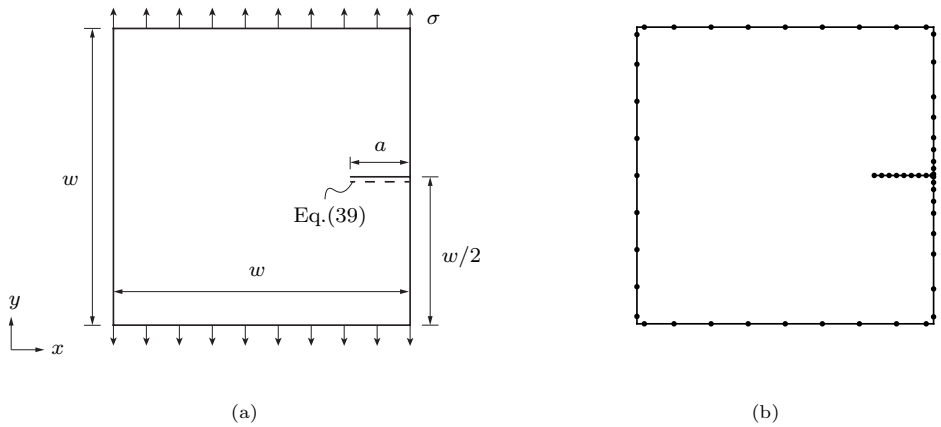

Figure 8: Square domain with an edge crack: (a) Geometry and loads: $a = w/5$; (b) Mesh.

additional boundary the interface conditions of continuity and equilibrium are enforced.

The problem is then solved using the formulation proposed in the present work. In particular, Eqs.(1) and (38) are used on the external boundary of the domain and on one side of the edge crack, respectively. On the remaining side crack of the crack, Eq.(39) is used, see Fig.(8a). The obtained results are shown Figs.(9a) and (9b) in the cases of isotropic and anisotropic behaviour, respectively .

The fourth test involves an internally cracked square domain. The domain is shown in Fig.(10a) and is loaded by uniform tractions over the top and bottom edges, whereas the remaining boundaries and the crack are traction-free. In this case, the presence of the internal crack makes the domain doubly-connected. The employed mesh of the domain is shown in Fig.(8b) where it is possible to notice that also in this case the crack tips are modelled as continuous. Although for the edge crack test the continuity of the crack

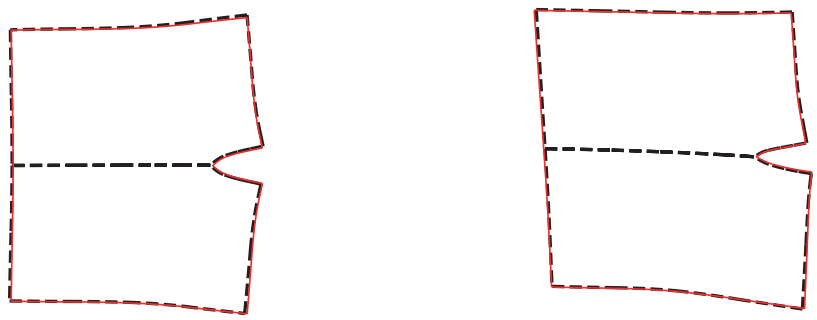

(a) (b)

Figure 9: Deformed shape of the square domain with an edge crack: (a) isotropic and (b) anisotropic.

tip is not required, in this case it is necessary since collocating Eq.(40) at the crack tips provides the additional equation that can be used to remove the additional unknown constant appearing in the alternative equation itself.

Also in this case, the analysis via the multi-region approach provides the reference solution, which is obtained by introducing two additional boundaries where the same interface conditions as the previous test are enforced.

The solution via the proposed formulation is then obtained by collocating Eqs.(1) and (38) on the external boundary of the domain and on one side of the edge crack, respectively, and Eq.(40) on the remaining side crack. Eq.(40) is also collocated at the crack tips to remove the additional constant. The obtained results are shown Figs.(11a) and (11b) in the cases of isotropic and anisotropic behaviour, respectively.

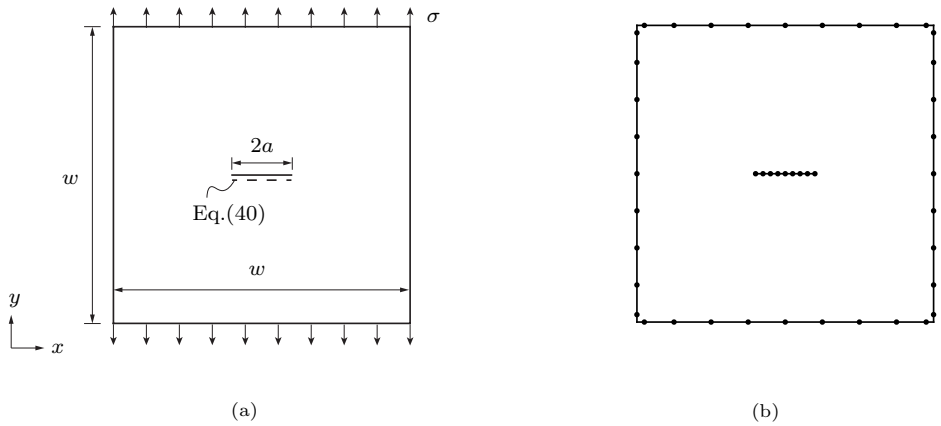

Figure 10: Square domain with a centered internal crack: (a) Geometry and loads $2a = w/5$; (b) Mesh.

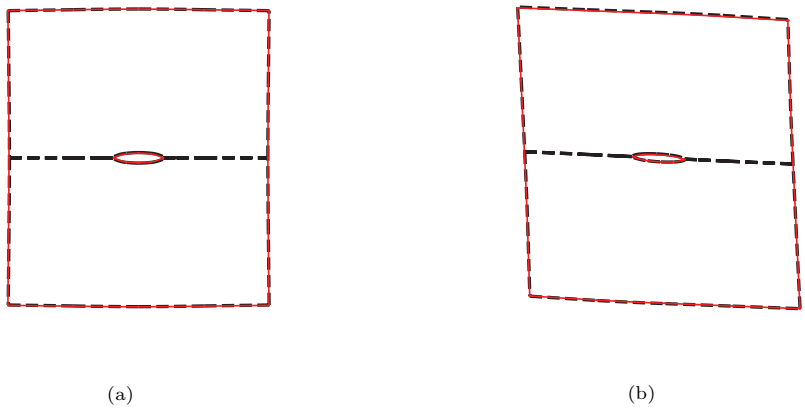

Figure 11: Deformed shape of the square domain with an internal crack: (a) isotropic; (b) anisotropic.

7.2. Stress Intensity Factor evaluation

To assess the accuracy of the proposed approach for fracture mechanics, the stress intensity factors in opening and sliding modes, namely K_I and K_{II}, are computed for several test cases and the obtained results are compared with reference values available in the literature. The stress intensity factors are evaluated using the path-independent M integral [31, 32] as briefly recalled in the following.

Considering the current BEM solution and an auxiliary solution $\{\boldsymbol{u}^{(i)}, \boldsymbol{\epsilon}^{(i)}, \boldsymbol{\sigma}^{(i)}\}$, the M integral is defined as

$$M^{(i)} = \int_{\gamma} \left(\widetilde{W}^{(i)} n_x - \boldsymbol{t}^{(i)T} \boldsymbol{u}_{,x} - \boldsymbol{t}^T \boldsymbol{u}_{,x}^{(i)} \right) \mathrm{d}S, \tag{46}$$

where γ is a generic contour that begins at one crack surface and ends at the opposite crack surface, $\boldsymbol{t}^{(i)}$ are the tractions defined on γ and associated to the auxiliary solution, and $\widetilde{W}^{(i)} \equiv \boldsymbol{\sigma}^{(i)T} \boldsymbol{\epsilon} = \boldsymbol{\sigma}^T \boldsymbol{\epsilon}^{(i)}$. Moreover, it is possible to show that the expression of the M integral can also be written as follows

$$M^{(i)} = 2\alpha_{11} K_I K_I^{(i)} + \alpha_{12}(K_I K_{II}^{(i)} + K_{II} K_I^{(i)}) + 2\alpha_{22} K_{II} K_{II}^{(i)}, \tag{47}$$

where the coefficients α_{11}, α_{12} and α_{22} are functions of the material properties and their expressions can be found in [31], K_I and K_{II} denote the stress intensity factors related to the BEM solution and $K_I^{(i)}$ and $K_{II}^{(i)}$ denote the stress intensity factors related to the auxiliary solution. Therefore, choosing two independent solutions $\{\boldsymbol{u}^{(1)}, \boldsymbol{\epsilon}^{(1)}, \boldsymbol{\sigma}^{(1)}\}$ and $\{\boldsymbol{u}^{(2)}, \boldsymbol{\epsilon}^{(2)}, \boldsymbol{\sigma}^{(2)}\}$ such that $\{K_I^{(1)}, K_{II}^{(1)}\} = \{1, 0\}$ and $\{K_I^{(2)}, K_{II}^{(2)}\} = \{0, 1\}$, and using Eq.(47), it is possible to write

$$M^{(1)} = 2\alpha_{11} K_I + \alpha_{12} K_{II} \tag{48a}$$

$$M^{(2)} = \alpha_{12} K_I + 2\alpha_{22} K_{II}. \tag{48b}$$

Eqs.(48a) and (48b) represents a system of equations that allows computing the stress intensity factors K_I and K_{II} under mixed mode crack opening conditions.

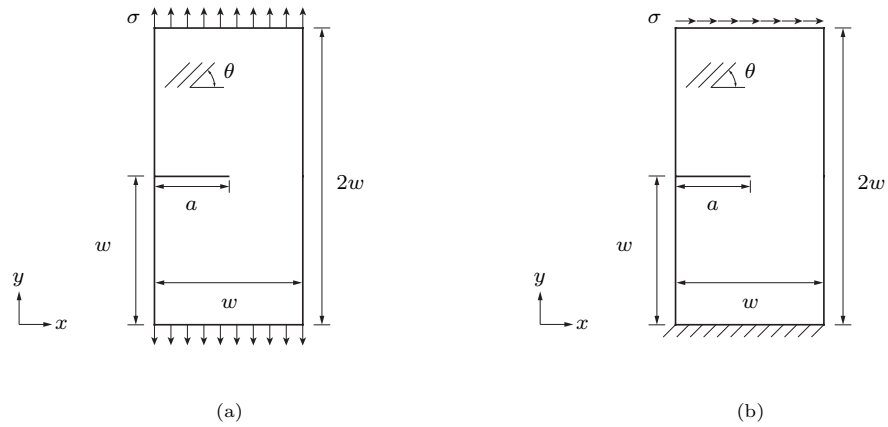

Figure 12: Geometry and loads for the two considered mixed-mode problems taken from Ref.[33]: (a) uniform traction problem and (b) cantilever plate problem. In the figures, $a = w/2$ and θ denotes the orientation of the material's axes with respect to the global reference system.

It is worth noting that the left-hand sides of Eqs.(48a) and (48b) are numerically evaluated using *i*) Eq.(46), *ii*) the BEM solution computed using the proposed formulation and *iii*) the explicit expression of the two auxiliary solutions, which can be found in [31].

In what follows, the above technique is employed to compute the stress intensity factors for a few test cases involving anisotropic material behaviors. For each test, the mesh size of the domain and the number of quadrature points to compute the M integral have been chosen to ensure the convergence and accuracy of the results.

In the first set of tests, a unidirectional graphite-epoxy rectangular lamina in presence of an edge crack is studied. Two different sets of boundary conditions, as shown in Fig.(12), are investigated. The material properties are taken from [33] and the stress intensity factors are computed as functions of the orientation of the material's principal

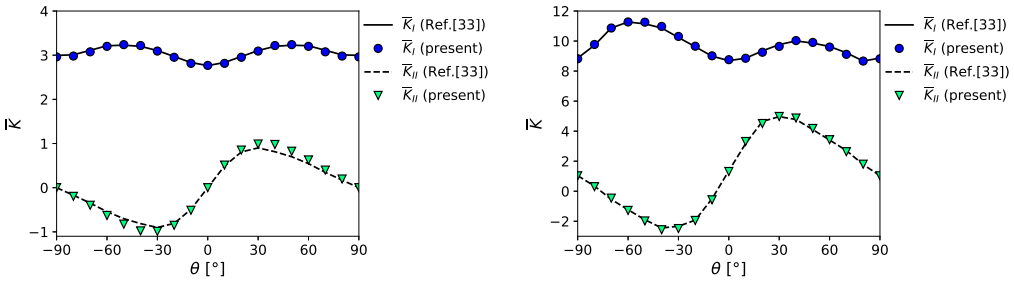

(a) (b)

Figure 13: Normalized stress intensity factors $\overline{K}_I \equiv K_I/(\sigma\sqrt{\pi a})$ and $\overline{K}_{II} \equiv K_{II}/(\sigma\sqrt{\pi a})$ as functions of the material orientation for the mixed-mode problems schematized in Fig.(12): (a) uniform traction problem and (b) cantilever plate problem.

axes. It is worth noting that, although the material is inherently orthotropic, its constitutive behavior in a reference system not aligned with the material's axes is characterized by a fully populated stiffness matrix.

The results corresponding to the boundary conditions shown in Figs.(12a) and (12b) are reported in Figs.(13a) and (13b), respectively, and are compared with those available in Ref.[33]. The obtained results corresponding to the boundary conditions shown in Figs.(12b) are also reported in Tab.(1) and show the accuracy of the proposed formulation.

In the second set of tests, the stress intensity factors are computed for one cracks and two cracks emanating from a hole centered in a unidirectional graphite-epoxy rectangular lamina subjected to a uniform traction as shown in Figs.(14a) and (14b), respectively.

Table 1: Stress intensity factors for an edge crack in a unidirectional graphite-epoxy laminate as functions of the fiber orientation.

θ	$K_I/(\sigma\sqrt{\pi a})$		$K_{II}/(\sigma\sqrt{\pi a})$	
	present	Ref.[33]	present	Ref.[33]
-90	8.8217	8.866	1.0265	1.037
-80	9.7720	9.721	0.3031	0.341
-70	10.8679	10.871	-0.4618	-0.547
-60	11.2718	11.269	-1.2776	-1.234
-50	11.2576	11.145	-1.9812	-1.899
-40	10.9754	10.871	-2.5628	-2.444
-30	10.3082	10.237	-2.4863	-2.336
-20	9.6571	9.621	-1.9458	-1.926
-10	9.0163	8.992	-0.5708	-0.501
0	8.7589	8.695	1.3141	1.358
10	8.8535	8.857	3.3110	3.171
20	9.2552	9.343	4.5087	4.646
30	9.6445	9.763	4.9782	4.966
40	10.0320	10.008	4.8746	4.778
50	9.9082	9.862	4.1799	4.101
60	9.6005	9.639	3.4310	3.410
70	9.1174	9.218	2.6321	2.707
80	8.6674	8.669	1.7990	1.775
90	8.8217	8.866	1.0265	1.037

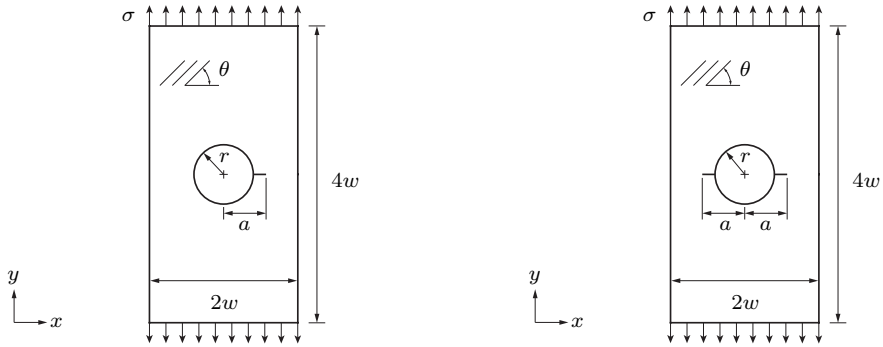

(a) (b)

Figure 14: Geometry and loads for the problems taken from Ref.[34]: (a) one crack and (b) two cracks emanating from a centered hole in a rectangular domain. In the figures, $r/w = 0.5$, $a/w = 0.7$ and θ denotes the orientation of the material's axes with respect to the global reference system.

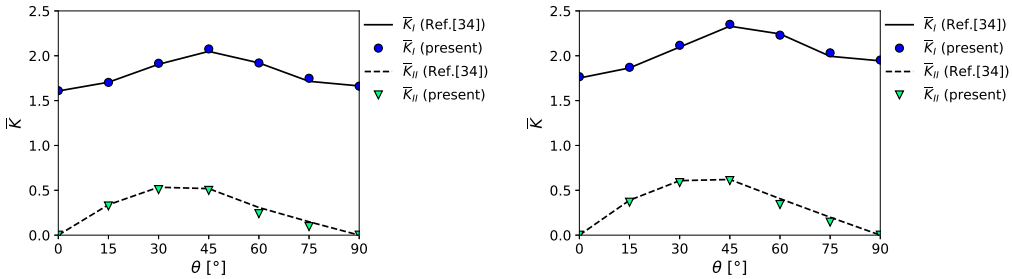

(a) (b)

Figure 15: Normalized stress intensity factors $\overline{K}_I \equiv K_I/(\sigma\sqrt{\pi a})$ and $\overline{K}_{II} \equiv K_{II}/(\sigma\sqrt{\pi a})$ as functions of the material orientation for the mixed-mode problems schematized in Fig.(14): (a) one-crack problem and (b) two-crack problem.

The material properties are taken from [34] and, similarly to the previous set of tests, the stress intensity factors are computed as functions of the orientation of the material's principal axes.

The results corresponding to the one-crack and to the two-crack problems are reported in Figs.(15a) and (15b), respectively, and are compared with those available in Ref.[34], showing, also in this case, the accuracy of the proposed formulation.

The reported tests show that the proposed formulation allows addressing fracture mechanics problems via a single region approach without the need of evaluating hyper-singular integrals.

8. Conclusions

A novel boundary element formulation for fracture mechanics of generally anisotropic two-dimensional bodies has been developed and numerically tested. The formulation is derived starting from the representation of the displacements as a linear superposition of a vector field, whose components satisfy a specifically defined anisotropic Laplace equation, and the gradient of the stress function. The sough supplementary boundary integral equation is then obtained using such displacement representation into the boundary integral representation of the mentioned anisotropic Laplace equation. The supplementary equation neither introduces hyper-singular integrals nor additional variables and allows the solution of two-dimensional anisotropic fracture problems in a single-region. Numeri-

cal results have been presented for simply- and doubly-connected cracked and uncracked domains and have been compared with those obtained by classic formulations, confirming the accuracy and potential of the proposed strategy.

References

[1] N. Moës, J. Dolbow, T. Belytschko, A finite element method for crack growth without remeshing, International journal for numerical methods in engineering 46 (1) (1999) 131–150. doi:10.1002/(SICI)1097-0207(19990910)46:1<131::AID-NME726>3.0.CO;2-J.

[2] C. Daux, N. Moës, J. Dolbow, N. Sukumar, T. Belytschko, Arbitrary branched and intersecting cracks with the extended finite element method, International journal for numerical methods in engineering 48 (12) (2000) 1741–1760. doi:10.1002/1097-0207(20000830)48:12<1741::AID-NME956>3.0.CO;2-L.

[3] N. Sukumar, D. Srolovitz, T. Baker, J.-H. Prévost, Brittle fracture in polycrystalline microstructures with the extended finite element method, International Journal for Numerical Methods in Engineering 56 (14) (2003) 2015–2037. doi:10.1002/nme.653.

[4] P. K. Banerjee, R. Butterfield, Boundary element methods in engineering science, Vol. 17, McGraw-Hill London, 1981.

[5] M. H. Aliabadi, The boundary element method, applications in solids and structures, Vol. 2, John Wiley & Sons, 2002.

[6] M. Snyder, T. Cruse, Boundary-integral equation analysis of cracked anisotropic plates, International Journal of Fracture 11 (2) (1975) 315–328. doi:10.1007/BF00038898.

[7] K. Chan, T. Cruse, Stress intensity factors for anisotropic compact-tension specimens with inclined cracks, Engineering Fracture Mechanics 23 (5) (1986) 863–874. doi:10.1016/0013-7944(86)90097-4.

[8] J. Telles, G. Castor, S. Guimaraes, A numerical green's function approach for boundary elements applied to fracture mechanics, International Journal for Numerical Methods in Engineering 38 (19) (1995) 3259–3274. doi:10.1002/nme.1620381906.

[9] G. E. Blandford, A. R. Ingraffea, J. A. Liggett, Two-dimensional stress intensity factor computations using the boundary element method, International Journal for Numerical Methods in Engineering 17 (3) (1981) 387–404. doi:10.1002/nme.1620170308.

[10] C. Tan, Y. Gao, Boundary element analysis of plane anisotropic bodies with stress concentrations and cracks, Composite Structures 20 (1) (1992) 17–28. doi:10.1016/0263-8223(92)90008-Z.

[11] G. Davì, A. Milazzo, Multidomain boundary integral formulation for piezoelectric materials fracture mechanics, International Journal of Solids and Structures 38 (40-41) (2001) 7065–7078. doi:10.1016/S0020-7683(00)00416-9.

[12] I. Benedetti, M. Aliabadi, A three-dimensional grain boundary formulation for microstructural modeling of polycrystalline materials, Computational Materials Science 67 (2013) 249–260. doi:10.1016/j.commatsci.2012.08.006.

[13] I. Benedetti, M. Aliabadi, A three-dimensional cohesive-frictional grain-boundary micromechanical model for intergranular degradation and failure in polycrystalline materials, Computer Methods in Applied Mechanics and Engineering 265 (2013) 36–62. doi:10.1016/j.cma.2013.05.023.

[14] V. Gulizzi, A. Milazzo, I. Benedetti, An enhanced grain-boundary framework for computational homogenization and micro-cracking simulations of polycrystalline materials, Computational Mechanics 56 (4) (2015) 631–651. doi:10.1007/s00466-015-1192-8.

[15] V. Gulizzi, C. Rycroft, I. Benedetti, Modelling intergranular and transgranular micro-cracking in polycrystalline materials, Computer Methods in Applied Mechanics and Engineering 329 (2018) 168 – 194. doi:https://doi.org/10.1016/j.cma.2017.10.005.

URL http://www.sciencedirect.com/science/article/pii/S0045782517306746

[16] I. Benedetti, V. Gulizzi, A. Milazzo, Grain-boundary modelling of hydrogen assisted intergranular stress corrosion cracking, Mechanics of Materials 117 (2018) 137 – 151. doi:https://doi.org/10.1016/j.mechmat.2017.11.001.
URL http://www.sciencedirect.com/science/article/pii/S0167663617305276

[17] A. Portela, M. H. Aliabadi, D. P. Rooke, The dual boundary element method: Effective implementation for crack problems, International Journal for Numerical Methods in Engineering 33 (6) (1992) 1269–1287. doi:10.1002/nme.1620330611.

[18] A. Portela, M. Aliabadi, D. P. Rooke, Dual boundary element incremental analysis of crack propagation, Computers & Structures 46 (2) (1993) 237–247. doi:10.1016/0045-7949(93)90189-K.

[19] P. Sollero, M. Aliabadi, Fracture mechanics analysis of anisotropic plates by the boundary element method, International Journal of Fracture 64 (4) (1993) 269–284. doi:10.1007/BF00017845.

[20] M. Aliabadi, P. Sollero, Crack growth analysis in homogeneous orthotropic laminates, Composites science and technology 58 (10) (1998) 1697–1703. doi:10.1016/S0266-3538(97)00240-6.

[21] E. Albuquerque, P. Sollero, M. Aliabadi, Dual boundary element method for anisotropic dynamic fracture mechanics, International Journal for Numerical Methods in Engineering 59 (9) (2004) 1187–1205. doi:10.1002/nme.912.

[22] N. Prasad, M. Aliabadi, D. Rooke, The dual boundary element method for thermoelastic crack problems, International Journal of Fracture 66 (3) (1994) 255–272. doi:10.1007/BF00042588.

[23] N. Prasad, M. Aliabadi, D. Rooke, The dual boundary element method for transient thermoelastic crack problems, International journal of solids and structures 33 (19) (1996) 2695–2718. doi:10.1016/0020-7683(95)00183-2.

[24] G. Geraci, M. Aliabadi, Micromechanical boundary element modelling of transgranular and intergranular cohesive cracking in polycrystalline materials, Engineering Fracture Mechanics 176 (2017) 351–374. doi:10.1016/j.engfracmech.2017.03.016.

[25] G. Geraci, M. Aliabadi, Micromechanical modelling of cohesive thermoelastic cracking in orthotropic polycrystalline materials, Computer Methods in Applied Mechanics and Engineering 339 (2018) 567–590. doi:10.1016/j.cma.2018.05.011.

[26] G. Davì, A. Milazzo, An alternative BEM for fracture mechanics, Structural Durability & Health Monitoring 2 (2006) 177–182.

[27] G. Davì, A. Milazzo, An alternative 2d BEM for fracture mechanics in orthotropic materials, Structural Durability & Health Monitoring 3 (4) (2007) 229–238.

[28] W.-L. Yin, Deconstructing plane anisotropic elasticity: Part i: The latent structure of Lekhnitskii's formalism, International Journal of Solids and Structures 37 (38) (2000) 5257 – 5276. doi:https://doi.org/10.1016/S0020-7683(99)00214-0.

[29] P. C. Chou, N. J. Pagano, Elasticity: tensor, dyadic, and engineering approaches, Courier Corporation, 1992.

[30] E. Lutz, W. Ye, S. Mukherjee, Elimination of rigid body modes from discretized boundary integral equations, International Journal of Solids and Structures 35 (33) (1998) 4427–4436. doi:10.1016/S0020-7683(97)00261-8.

[31] J. K. Knowles, E. Sternberg, On a class of conservation laws in linearized and finite elastostatics, Archive for rational mechanics and analysis 44 (3) (1972) 187–211.

[32] F. H. Chen, R. T. Shield, Conservation laws in elasticity of the j-integral type, Zeitschrift fuer angewandte Mathematik und Physik 28 (1) (1977) 1–22.

[33] S. Chu, C. S. Hong, Application of the Jk integral to mixed mode crack problems for anisotropic composite laminates, Engineering Fracture Mechanics 35 (6) (1990) 1093–1103.

[34] P. Sollero, M. Aliabadi, D. Rooke, Anisotropic analysis of cracks emanating from cir-

cular holes in composite laminates using the boundary element method, Engineering fracture mechanics 49 (2) (1994) 213–224.